Unique Activity of Platinum Adislands in the CO Electrooxidation Reaction

ARTICLE *in* JOURNAL OF THE AMERICAN CHEMICAL SOCIETY · NOVEMBER 2008

Impact Factor: 12.11 · DOI: 10.1021/ja8032185 · Source: PubMed

J|A|C|S
ARTICLES

Unique Activity of Platinum Adislands in the CO Electrooxidation Reaction

Dusan S. Strmcnik,[†] Dusan V. Tripkovic,[†] Dennis van der Vliet,[†] Kee-Chul Chang,[†] Vladimir Komanicky,[†] Hoydoo You,[†] Goran Karapetrov,[†] Jeffrey P. Greeley,[‡] Vojislav R. Stamenkovic,[†] and Nenad M. Marković*,[†]

Materials Science Division and Center for Nanoscale Materials, Argonne National Laboratory, Argonne, Illinois 60439

Received April 30, 2008; E-mail: nmmarkovic@anl.gov

Abstract: The development of electrocatalytic materials of enhanced activity and efficiency through careful manipulation, at the atomic scale, of the catalyst surface structure has long been a goal of electrochemists. To accomplish this ambitious objective, it would be necessary both to obtain a thorough understanding of the relationship between the atomic-level surface structure and the catalytic properties and to develop techniques to synthesize and stabilize desired active sites. In this contribution, we present a combined experimental and theoretical study in which we demonstrate how this approach can be used to develop novel, platinum-based electrocatalysts for the CO electrooxidation reaction in CO(g)-saturated solution; the catalysts show activities superior to any pure-metal catalysts previously known. We use a broad spectrum of electrochemical surface science techniques to synthesize and rigorously characterize the catalysts, which are composed of adisland-covered platinum surfaces, and we show that highly undercoordinated atoms on the adislands themselves are responsible for the remarkable activity of these materials.

Introduction

In 1925, H. S. Taylor proposed that a few sites on catalyst surfaces might be uniquely active for catalytic reactions.[1] Today, although significant progress has been made in elucidating the nature of these so-called "active sites" in gas-phase catalytic systems, their structure in electrochemical environments remains largely elusive even for the simplest reactions, such as the electrooxidation of carbon monoxide on platinum ($CO_{ad} + OH_{ad} = CO_2 + H^+ + e^-$). This reaction serves as a model reaction in the electrocatalysis of small organic molecules,[2,3] and it is relevant to a variety of fundamental and technological applications, including the search for CO-tolerant hydrogen oxidation catalysts.[4,7] Studies in ultrahigh vacuum environments have shown that the oxidative removal of adsorbed CO occurs via reaction between oxygen chemisorbed preferentially on step sites and CO adsorbed on terrace sites.[8] Corresponding electrochemical studies on stepped Pt single crystal surfaces focused on so-called CO stripping curves produced by the electrooxidation of one monolayer of preadsorbed CO in a solution saturated with inert gases. The current peaks were found to shift toward more negative potentials with increasing step density.[9,10] Based on this observation and in line with gas-phase catalysis, it was proposed that the electrochemical adsorption of hydroxyl species (hereafter denoted as OH_{ad}) is enhanced on step sites and that the CO electrooxiadtion reaction proceeds between this OH_{ad} and CO adsorbed on terrace sites.[10] However, in stripping studies, attention has been focused almost exclusively on the position of CO stripping peaks (which may be analogous to the so-called ignition potential in CO bulk experiments[11]), and the nature of the active sites in the so-called preignition potential region has not been considered. The term "preignition potential" was originally coined to describe the small currents in CO-saturated (bulk) solution that are seen at potentials well below the ignition potential. It is important to emphasize that it is the preignition region that determines the anode performance in practical hydrogen fuel cells where the feed consists of H_2 plus CO contaminants; relatively modest CO oxidation currents in this region can free sufficient surface sites to produce robust hydrogen oxidation rates.[3] Hence, the understanding of the active sites that are responsible for the preignition region is of paramount importance for the development of improved electrocatalysts.

In the present work, we use a combination of experimental and theoretical techniques, including electrochemical (EC), scanning tunneling microscopy (STM), infrared adsorption

[†] Materials Science Division.
[‡] Center for Nanoscale Materials.

(1) Taylor, H. S. *Proceedings of the Royal Society of London, Series A*; The Royal Society: 1925; Vol. 108, p 105.
(2) Jarvi T. D.; Stuve, E. M. *Electrocatalysis*; Wiley-VCH, Inc.: New York, 1998; Chapter 3, pp 75−153.
(3) Markovic, N. M.; Ross, P. N. *Surf. Sci. Rep.* **2002**, *45*, 117–230.
(4) Hamnett, A. *Philos. Trans. R. Soc. London, Ser. A* **1996**, *354*, 1653–1669.
(5) Markovic, N. M.; Ross, P. N. *Cat. Tech.* **2000**, *4*, 110–126.
(6) Vielstich, W.; Lamm. A.; Gasteiger, H. A. *Handbook of Fuel Cells, Fundamentals Technology and Applications*; John Wiley & Sons Ltd.: West Sussex, 2003.
(7) Russell, A. E.; Rose, A. *Chem. Rev.* **2004**, *104*, 4613–4635.
(8) Xu, J.; Jates, J. T. *J. Chim. Phys.* **1993**, *99*, 725.
(9) Lebedeva, N. P.; Koper, M.; Herrero, E.; Feliu, J. M.; van Santen, R. A. *J. Electroanal. Chem.* **2000**, *487*, 37–44.
(10) Lebedeva, N. P.; Rodes, A.; Feliu, J. M.; Koper, M. T. M.; van Santen, R. A. *J. Phys. Chem. B* **2002**, *106*, 9863–9872.
(11) Markovic, N. M.; Lucas, C.; Grgur, B. N.; Ross, P. N. *J. Phys. Chem.* **1999**, *103*, 9616–9623.

10.1021/ja8032185 CCC: $40.75
Published on Web 10/23/2008

spectroscopy (IRAS), and density functional theory (DFT), to determine the nature of the active sites for bulk CO electrooxidation in the preignition potential region. We demonstrate that these sites are highly undercoordinated platinum adislands (size range 0.5−4.0 nm), formed as a consequence of removing (lifting) surface reconstructions,[12] and that they are substantially more active than pure step sites. We note that, to be consistent with standard nomenclature in electrocatalysis,[13] we define the electrocatalytic activity of all Pt(hkl) surfaces for bulk CO oxidation as the current per unit surface area measured at fixed potential; this definition implies that the reported activity is averaged over sites both with and without adsorbed CO. In some cases, the measured activities on the adislands approach the best CO electrooxidation rates ever obtained on state-of-the-art transition metal bimetallic catalysts. We determine that this increased activity is closely related to a delicate balance between CO and OH adsorption on the platinum surfaces; we find that OH competes better with CO for adsorption sites on the adislands than it does on other surface features, leading to the remarkable activity. The interplay between OH and CO, in turn, leads to a dynamic evolution of the surface morphology over the course of the reaction; the destruction of the adislands leads to a sharp decrease in rate, but these important nanostructures can be stabilized if the potential is kept below the CO electrooxidation ignition potential. We anticipate that the remarkable surface activity shown by these nanostructural features will be transferable to a variety of other metals and electrochemical reactions. In effect, by carefully controlling the active sites of electrocatalytic surfaces in a manner similar to that used in the present study, it may be possible to synthesize novel electrocatalysts with substantially enhanced activity and improved catalytic properties.

Experimental Section

The basic tactics employed here involve measuring electrooxidation rates for CO bulk electrooxidation as a function of the applied positive potential limits as well as the number of potential cycles and then (i) recording cyclic voltammograms in Ar saturated solutions; (ii) determining CO vibrational properties (ν_{CO}) and reactivity (CO_2 production, I_{CO2}) by IRAS spectra; (iii) extracting corresponding STM images; and (iv) (after the step (iii)) checking the cyclic voltammetry in an electrochemical cell purged with Ar.

The platinum single crystals were prepared by inductive heating for 30 min at ∼1300 K in an argon hydrogen flow (3% hydrogen). The annealed specimens were cooled slowly to room temperature in this flow stream and immediately covered by a droplet of water *saturated with hydrogen*. The electrodes were then embedded into the rotating disk electrode (RDE) and transferred into the electrochemical cell. The electrode was always immersed in electrolyte at 0.05 V. In the CO experiments, the electrolyte was always equilibrated with CO at 0.05 V. Subsequent data were acquired on electrodes either *without* any prior potential cycling (in the text denoted as the "as-prepared" electrode) or after 20 potential cycles to 0.75 and 0.95 V in CO-saturated solution (in the text denoted as the "CO-annealing" method). We selected this protocol because we found that 20 potential cycles were sufficient to change the surface morphology and catalytic activity in such a way that all techniques (see below) could capture the essence of the effects of adislands and steps on the catalytic activity of Pt single crystal surfaces. We emphasize that, after each set of cycles to 0.75 or 0.95 V, the electrodes were freshly prepared before subsequent electrochemical testing was performed. Although all polarization curves are reported for sweep rates of 50 mV/s, the same order of activity for the different single crystal facets was obtained at much lower sweep rates (1 mV/s). All potentials are referenced to the potential of the reversible hydrogen electrode.

The experimental STM procedure for characterizing the morphology of the as-prepared and CO-annealed surfaces involved several steps. First, after the electrochemical pretreatment described above, electrodes covered with CO were emersed from the CO-saturated electrolyte at 0.05 V, transferred to a glovebox filled with CO, and mounted on a microscope which was then enclosed in an airtight cylinder filled with CO at 1 atm.[14] During the experiments, the partial pressure inside the cylinder was varied by overpressurizing the cylinder with a known amount of high-purity Ar or CO. STM images were acquired with a Digital Instrumentations Multi-Mode Dimension STM controlled by a Nanoscope III control station. In the STM experiments, the "$\sqrt{19}$" structure (see Supporting Information and refs 15 and 16), seen on terraces of all three Pt(111) surfaces (Figure 2a−c), was observed by diluting the CO atmosphere with Ar so that the CO content in a cylinder was ∼70%; use of a pure CO atmosphere, on the other hand, can yield a (2 × 2)-3CO structure. In the case of Pt(100), no CO structure was seen under any experimental conditions. After the STM characterization, the CO-covered electrode was transferred back into the electrochemical cell purged with Ar. Following stripping of CO_{ad}, voltammograms were recorded in the second potential sweep. For all results presented in this paper, the voltammograms *before* and *after* STM measurements were identical, suggesting that during STM experiments the electrode stays clean.

The experimental IRAS protocol for characterizing both the ν_{CO} vs E, as well as the I_{CO2} vs E relationships, on the as-prepared and CO-annealed surfaces involved electrode transfer directly from the RF apparatus into the IRAS spectroelectrochemical cell designed for an external reflection mode in a thin layer configuration. A Nicolet Nexus 670 spectrometer was available, equipped with a liquid-N_2 cooled MCT detector. Before data acquisition, the electrode pretreatment was identical to that described for the electrochemical measurements. Prior to each measurement, the solution was saturated with CO for at least 3 min, holding the electrode potential at 0.05 V. All IR measurements were performed in a spectroelectrochemical glass cell designed for an external reflection mode in a thin layer configuration. The cell is coupled at its bottom with a CaF_2 prism beveled at 60° from the prism base (for a schematic representation of the spectroelectrocehmical cell, see ref 17). The spectra were recorded with a resolution of 8 cm^{-1}. All measurements were performed using p-polarized light. To obtain a single beam spectrum, 50 scans were collected at each potential, resulting in a recording time of 25 s. Absorbance spectra were calculated as the ratio $-\log(R/R_0)$, where R and R_0 are the reflectance values corresponding to the sample and reference spectra, respectively. Reference spectra were recorded at 0.9 V, where CO_{ad} is completely oxidized, or at −0.05 V, where a compact CO adlayer is present on the surface. For more details, see refs 18 and 19.

The DACAPO code[20] was used for all total energy calculations in this study. For calculations on both the perfect Pt(111) terraces and the terraces with adatoms present, three-layer slabs, periodically repeated in a super cell geometry with seven equivalent layers of vacuum between any two successive metal slabs, were used. To

(12) Kibler, L. A.; Cuesta, M.; Kleinert, M.; Kolb, D. M. *J. Electroanal. Chem.* **2000**, *484*, 73–82.
(13) Bockris, J. O. M.; Reddy, A. K. N. *Modern Electrochemistry*; Plenum Press: New York, 1970.
(14) Menzel, A.; Chang, K.-C.; Komanicky, V.; Tolmachev, Y. V.; Tkachuk, A.; Chu, S. Y.; You, H. *Phys. Rev. B* **2007**, *75*, 0345426.
(15) Villegas, I.; Weaver, M. J. *J. Chem. Phys.* **1994**, *101*, 1648.
(16) Tolmachev, Y. V.; Menzel, A.; Tkachuk, A.; Chu, S. Y.; You, H. *Electrochem. Solid-State Lett.* **2004**, *7*, E23.
(17) Stamenkovic, V.; Arenz, M.; Ross, P. N.; Markovic, N. M. *J. Phys. Chem. B* **2004**, *108*, 17915–17920.
(18) Stamenkovic, V.; Arenz, M.; Lucas, C.; Gallagher, M.; Ross, P. N.; Markovic, N. M. *J. Am. Chem. Soc.* **2003**, *125*, 2736–2745.
(19) Stamenkovic, V.; Chou, K. C.; Somorjai, G. A.; Ross, P. N.; Markovic, N. M. *J. Phys. Chem. B* **2005**, *109*, 678–680.

capture the subtle relaxations that occur when defects are introduced into the high-coverage CO adlayer, a (4 × 4) unit cell was employed. In all calculations, the high-coverage CO states were modeled by a (2 × 2)-3CO structure, allowing for perturbations near the adatoms and step edges (see Supporting Information). To evaluate the stabilizing effect of a water bilayer on an OH molecule coadsorbed on an adatom with a CO molecule, a smaller unit cell (3 × 2 - closely matching the natural periodicity of water bilayers), with two CO molecules on the terraces between the adatoms optimized in on-top geometries, was employed.[21] A similar approach was used to demonstrate that no water stabilization is expected on CO-covered perfect Pt(111) terraces or on CO-covered Pt(211) surfaces. For the Pt(211) calculations, a (3 × 4) unit cell was used; a total of nine layers were included. On the Pt(111) surfaces, both with and without adatoms, the top layer of the slab was allowed to relax until the total force on all atoms was less than 0.04 eV/Å in any Cartesian direction; on the Pt(211) surfaces, four layers were relaxed. In all cases, adsorption was allowed on one of the two exposed surfaces of the metal slabs, and the electrostatic potential was adjusted accordingly.[22] Ionic cores were described by ultrasoft pseudopotentials,[23] and the Kohn−Sham one-electron valence states were expanded in a basis of plane waves with a kinetic energy below 340 eV; a density cutoff of 500 eV was used. The surface Brillouin zone of the (4 × 4) unit cells was sampled with a (2 × 2 × 1) Monkorst−Pack **k** point grid, the (3 × 2) cell used a (3 × 4 × 1) **k** point grid, and the (3 × 4) cells used a (3 × 2 × 1) **k** point grid. The convergence of the total energy with respect to the cutoff energies and the **k** point set was confirmed. The exchange-correlation energy and potential were described by the generalized gradient approximation (GGA-RPBE).[20] The self-consistent RPBE density was determined by iterative diagonalization of the Kohn−Sham Hamiltonian, Fermi population of the Kohn−Sham states (k_BT = 0.1 eV), and Pulay mixing of the resulting electronic density.[24] All total energies were extrapolated to k_BT = 0 eV.

The approach for incorporating potential and entropy effects (at pH = 0) into the calculations of the free energy of adsorption for water splitting and concomitant OH adsorption has been described previously;[21,25] more details can be found in the Supporting Information.

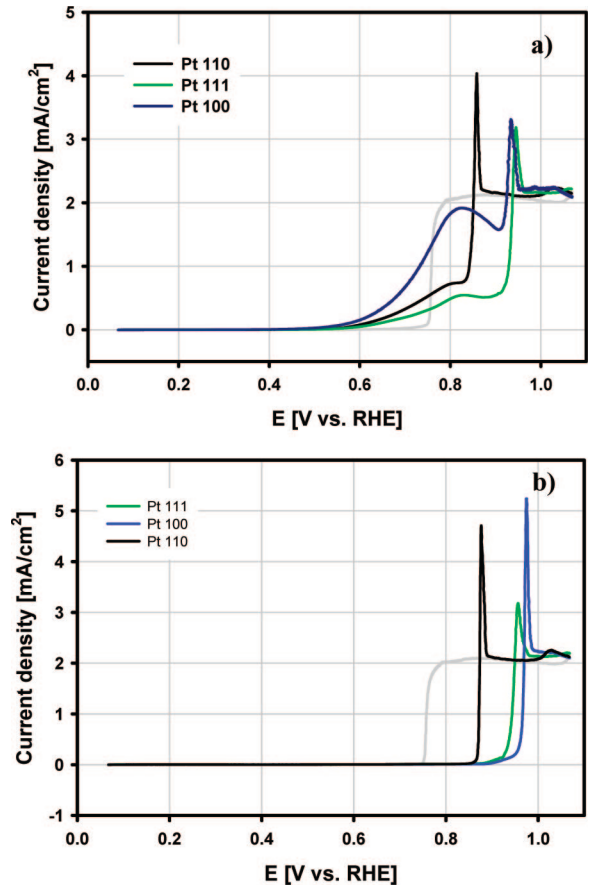

Figure 1. Polarization curves for CO bulk electrooxidation on Pt(100), Pt(111), and Pt(110) in 0.1 M $HClO_4$ recorded at 50 mV/s during (a) the first positive potential cycle to 1.1 V on the as-prepared electrodes and (b) the second consecutive sweep on the CO-annealed electrodes. Gray lines represent structure insensitive CO electrooxidation currents on the reverse sweeps.

Results and Discusion

We begin with a description of polarization curves for CO electrooxidation on low-index Pt single crystal surfaces in CO-saturated solutions (bulk CO electrooxidation). In our discussion, we emphasize the importance of the potential prehistory of the electrode in evaluating structure−function relationships; in previous studies on similar systems, the prehistory was not scrutinized in detail.[9−11] Figure 1 shows polarization curves obtained during the first (Figure 1a) and the second (Figure 1b) potential sweeps up to 1.1 V on Pt(100), Pt(111), and Pt(110) in 0.1 M $HClO_4$. Two potential regions can be distinguished in the first sweep (Figure 1a): modest rates at low overpotentials in the preignition potential region and rapid rates at the ignition potential[26,27] (the rate becomes entirely mass transfer limited above the ignition potential). The activity at the ignition potential increases in the order (100) ≈ (111) < (110), suggesting that steps or ridges (as are found in abundance on Pt(110)) may serve as the active sites within this potential regime, consistent with previous findings.[9,10] We note that, in the indicated references, the authors only analyzed structure sensitivity in the ignition potential region. However, as discussed above, it is the preignition region that is relevant for practical fuel cell anodes;[3] hence, we will focus exclusively on structure sensitivity in this regime in the following.

In contrast to the observed structure sensitivity at the ignition potential during the first potential sweep, the activity in the preignition region increases in the order (111) < (110) ≪ (100). These results indicate that a fully stepped (110) = 2(111) × (111) surface is not, in fact, the most active in this catalytically important region. In particular, at 0.8 V, the CO electrooxidation rate on Pt(100) is very close to the diffusion limiting value and is more than doubled with respect to Pt(110). Such high activity has never been observed previously on any Pt(*hkl*) surfaces under any experimental conditions. The question naturally arises as to what particular surface features are responsible for these activity trends and, in particular, which features permit the unique catalytic activity of Pt(100) in the preignition potential

(20) Hammer, B.; Hansen, L. B.; Norskov, J. K. *Phys. Rev. B* **1999**, *59*, 7413–7421.
(21) Norskov, J. K.; Rossmeisl, J.; Logadottir, A.; Lindqvist, L.; Kitchin, J. R.; Bligaard, T.; Jonsson, H. *J. Phys. Chem. B* **2004**, *108*, 17886–17892.
(22) Bengtsson, L. *Phys. Rev. B* **1999**, *59*, 12301–12304.
(23) Vanderbilt, D. *Phys. Rev. B* **1990**, *41*, 7892–7895.
(24) Kresse, G.; Furthmuller, J. *Phys. Rev. B* **1996**, *54*, 11169–11186.
(25) Stamenkovic, V.; Mun, B. S.; Mayrhofer, K. J. J.; Ross, P. N.; Markovic, N. M.; Rossmeisl, J.; Greeley, J.; Norskov, J. K. *Angew. Chem.* **2006**, *45*, 2897–2901.
(26) Markovic, N. M.; Grgur, B. N.; Lucas, C. A.; Ross, P. N. *J. Phys. Chem. B* **1999**, *103*, 487–495.
(27) Markovic, N. M.; Schmidt, T. J.; Grgur, B. N.; Gasteiger, H. A., Jr.; Behm, R. J. *J. Phys. Chem. B* **1999**, *103*, 8568–8577.

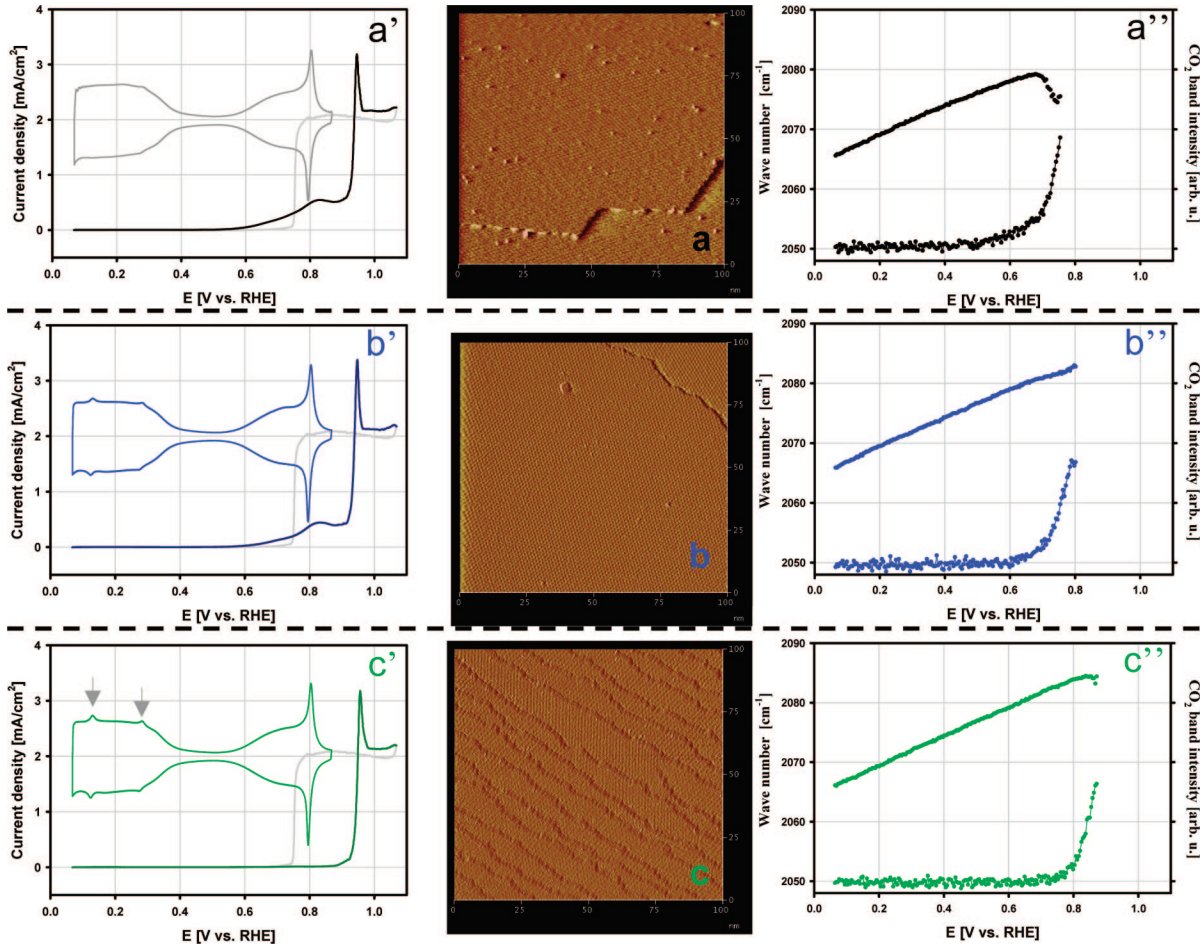

Figure 2. STM images (100 × 100 nm^2 size) of Pt(111) covered by CO for (a) as-prepared electrode and CO-annealed electrodes (20 consecutive cycles) to (b) 0.75 V and (c) to 0.95 V. The images (U_{tip} = 0.15 V; I_{tip} = 1 nA) illustrate the presence of islands and steps on the surface. Corresponding (a′−c′) cyclic voltammograms and polarization curves for CO bulk electrooxidation recorded at 50 mV/s in positive sweep direction (gray lines represent CO electrooxidation at negative sweep directions) and (a″−c″) potential dependent CO vibrational frequencies (upper part) and CO_2 intensities (lower part) obtained in IRAS experiments. Prolonged cycles (100 consecutive sweeps) to 0.75 V are needed to induce the step formation and concomitantly cease the activity in the preoxidation region, indicating that the potential prehistory is determining surface morphology and activity.

region. The resolution of this question, together with the related question of what surface morphological changes lead to the disappearance of the preignition region during the *second* potential sweep on all three Pt(*hkl*) surfaces (Figure 1b), could provide the fundamental understanding necessary to "engineer" active sites in electrocatalytic systems and to thereby develop CO electrooxidation catalysts of superior activity and stability.

To understand the relationship between the atomic-level surface morphological features in the preignition potential region and the remarkable electrocatalytic activity of Pt(100), we perform extensive structural measurements with STM, cyclic voltammetry, and CO vibrational spectroscopy; subsequently, we discuss results from additional probes of CO electrooxidation activity, including polarization curve measurements, CO_2 vibrational spectra, and DFT calculations. To probe the extremes of CO electrooxidation activities, we restrict our presentation to the most active (100) surfaces and the least active (111) surfaces.

STM images for Pt(111) and Pt(100) are presented in Figures 2a−c and 3a−c, respectively; the images were acquired on electrodes both without potential cycling and after applying 20 potential cycles, in a CO-saturated solution, to 0.75 and 0.95 V (see Experimental Section). The image of the as-prepared Pt(111) electrode (Figure 2a) reveals that the surface is composed of a flat terrace which is covered by adislands with monatomic height; the average width of the adislands is 1.5nm, corresponding to ~5 atoms or less. These features are even more evident on the as-prepared Pt(100) electrode (Figure 3a); the STM image shows roughly 15 times more adislands than on Pt(111) (see also Supporting Information), which is in agreement with the previous STM results.[12,28] The presence of such islands on the (111) and (100) surfaces is likely due to lifting of reconstructions of the thermally annealed surfaces.[3,29] On both surfaces, no change is seen in the adisland morphology when the potential is kept below 0.4 V. A modest reduction in the number and size of the islands is observed after CO annealing within the preignition region, as depicted in Figures 2b and 3b for potential excursions to 0.75 V (see Supporting Information). It is only after CO annealing to 0.95 V, however, that the adislands completely disappear (Figures 2c and 3c) and, in the case of Pt(111), are replaced by a series of smooth terrace-step structures; the steps have monatomic height and are located either on parallel lines or on lines forming angles of 120°. These features are more fully resolved in Figure 4a. Therein, it is

(28) Lopez-Cudero, A.; Cuesta, A.; Gutierrez, C. *J. Electroanal. Chem.* **2006**, *586*, 204–216.
(29) Grubel, G.; Huang, K. G.; Gibbs, D.; Zehner, D. M.; Sandy, A. R.; Mochrie, S. G. J. *Phys. Rev. B* **1993**, *48*, 18119–18139.

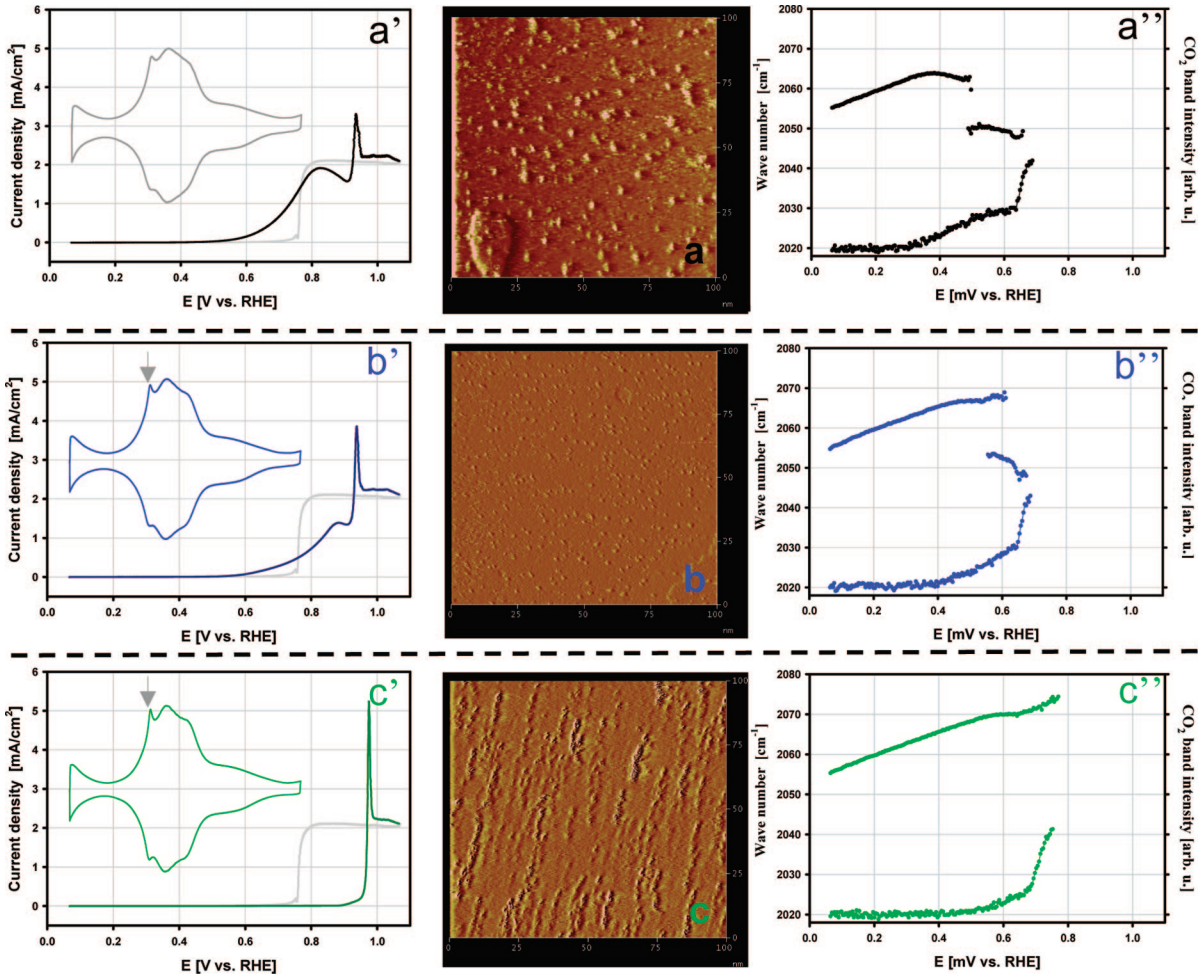

Figure 3. STM images (100 × 100 nm^2 size) of Pt(100) covered by CO for (a) as-prepared electrode and CO-annealed electrodes (20 consecutive cycles) to (b) 0.75 V and (c) to 0.95 V. The images (U_{tip} = 0.2 V; I_{tip} = 0.9 nA) illustrate the presence of adislands (a and b) and step-like formation on the surface cycled to 0.95 V (c). Corresponding (a′−c′) cyclic voltammograms and polarization curves for CO bulk electrooxidation recorded at 50 mV/s in the positive sweep direction (gray lines represent CO electrooxidation at negative sweep directions) and (a″−c″) potential dependent CO vibrational frequencies (upper part) and CO_2 intensities (lower part) obtained in IRAS experiments. As for Pt(111), 100 consecutive sweeps to 0.75 V are required to cease the activity in the preoxidation region.

evident that true, step-like features have formed and that all adislands have disappeared; it is further evident that these features show no activity for CO electrooxidation in the critical preignition potential region (polarization curves in Figures 2c′ and 3c′). In the case of Pt(100), CO annealing up to 0.95 V lead to the formation of stretched islands or step-like ridges (Figures 3c and 4b) in the long-periodicity direction of the hex-reconstruction, indicating that adatoms diffuse along this direction. These ridge-like features, although not perfect steps, are very large (typically 10 nm or more in length), and hence the average coordination number of the platinum atoms in these ridges is larger than that of platinum atoms in the adislands.

On both Pt(111) and Pt(100), since the transformation to step-/ridge-like features only occurs above the ignition potential for CO electrooxidation, we conclude that it is the CO electrooxidation reaction, as opposed to simple CO adsorption, that leads to step/ridge formation. We further note, in passing, that potential cycling to 0.95 V in CO-free solution leads to the formation of large adislands with di- and triatomic heights that are randomly distributed over the terraces (Supporting Information and ref 30). The absence of step formation in this case indicates that CO_{ad}, when present, acts as a surfactant that transports adatoms from terraces to steps. Step formation therefore appears to involve a delicate balance between the tendency of adsorbed oxygenated species to induce adisland formation at high potentials and the contrasting tendency of CO_{ad} to facilitate diffusion of adatoms/adislands across the surface with concomitant incorporation into step edges.

To gain further insight into the morphological characteristics of Pt surfaces under conditions relevant to CO electrooxidation, we examine the link between the STM-determined microscopic structures and corresponding features in cyclic voltammetry (CV) of Pt(111) and Pt(100). After CO annealing to 0.95 V, the size of hydrogen adsorption peaks (arrows in Figures 2c′ and 3c′) increases slightly relative to the surfaces that do not show steps in the STM scans, signaling the adsorption of hydrogen (H_{ad}) on step sites.[12,31,32] CVs of the as-prepared Pt(111) and Pt(100) surfaces (Figures 2a′ and 3a′) suggest that the electrodes are "well-ordered";[31−35] the obvious *disorder* evident in the STM scans, however, implies that the voltam-

(30) Sashikata, K.; Furuya, N.; Itaya, K. *J. Vac. Sci. Technol., A* **1991**, *B9*, 457.
(31) Markovic, N. M.; Marinkovic, N. S.; Adzic, R. R. *J. Electroanal. Chem.* **1988**, *241*, 309.
(32) Clavilier, J.; Rodes, A.; El-Achi, K.; Zamakhchari, M. A. *J. Chim. Phys.* **1991**, *88*, 1291–1337.
(33) Clavilier, J. *J. Electroanal. Chem.* **1980**, *107*, 211–216.
(34) Clavilier, J.; Armand, D.; Sun, S. G.; Petit, M. *J. Electroanal. Chem.* **1986**, *205*, 267–277.

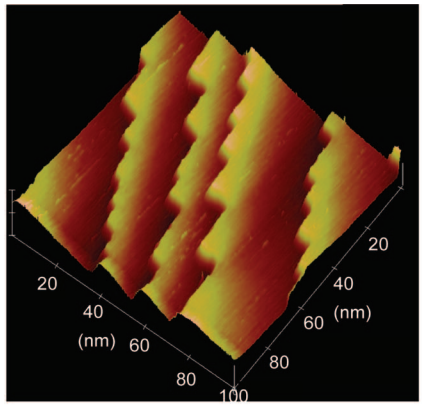

a)

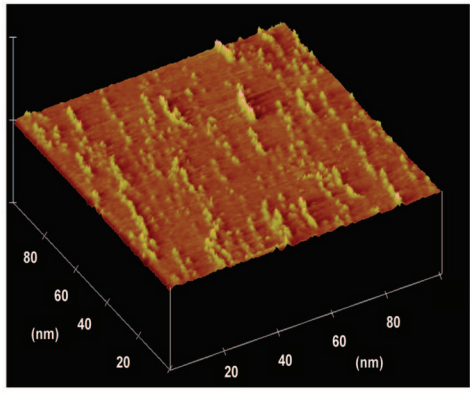

b)

Figure 4. Three dimensional STM topography of CO-annealed (up to 0.95 V) Pt(111) (a) and Pt(100) (b) in 0.1 $HClO_4$ solution ($U_{tip} = 0.2$ V, $I_{tip} = 0.9$ nA).

metric measurements are blind to the presence of adislands on the as-prepared surfaces. Intriguingly, then, while voltammetry appears to be a reliable method of detecting steps, it does not detect adislands.

To find an electrochemical method capable of seeing the adislands, we used IRAS to probe how the applied potential affects the vibrational properties of linearly bonded CO (ν_{CO}, Figures 2a″−c″ and 3a″−c″). Since ν_{CO} depends on both surface bonding and the local environment, we anticipate that it will provide information about surface morphology.[18,19,37−39] On Pt(100), indeed, the ν_{CO} signal clearly splits when a high density of adislands is present. However, a normal Stark tuning slope is found for a (100) surface free of adislands (Figure 3c″), suggesting that the appearance of two terminal-CO bands might be used as a diagnostic probe for adislands on this surface. In general, at the metal−liquid interface, the splitting of CO vibrational bands is a fairly common phenomenon. It is observed, for example, during adsorption of CO on Pt stepped single crystal surfaces covered by submonolayers of CO,[36−38] on some bimetallic surfaces at which CO is adsorbed on either both elemental components[40,41] or on only one of two components,[18] and on more oxophilic metals than Pt (e.g., on a Rh electrode[42] and the Pd(111) surface[43]). On the other hand, in accordance with Kim and Korzeniewski,[38] splitting is not seen at low potentials (saturation CO coverages) where dipole coupling is strong. It is thus seen that CO peak splitting may result, in general, from a rich spectrum of geometric and chemical factors. In the case of adislands, it is likely that, at higher potentials, the splitting of CO bands coincides with OH adsorption and CO electrooxidation on the more oxophilic adislands; these processes may affect the coupling of neighboring CO molecules on the adislands and "terraces", leading to a separation of the peak for adisland-bound CO (the low-energy mode at ~2050 cm^{-1}) from the peak for CO on the terrace (the high-energy mode at ~2065 cm^{-1}). The fact that the splitting of ν_{CO} is not observed for Pt(111) is presumably due to the lower concentration of adislands on this surface (see also Supporting Information).

Significantly, on all surfaces, deviations from linearity in the CO frequency versus potential curve coincide with the appearance of CO_2 signals (Figures 2a″−c″ and 3a″−c″) which, in turn, can be used as a probe of CO electrooxidation activity. Two findings are noteworthy. First, the activity in the preignition potential region always decreases when the number of adislands decreases and the step density increases. Second, the as-prepared (100) surface is highly active, with the onset of CO electrooxidation appearing as low as ~0.3 V. This activity is unique for pure Pt catalysts and is very close to the catalytic activity of the best bulk CO electrooxidation bimetallic catalysts, such as Pt−Ru,[44] Pt−Sn,[45] and Pt−Mo.[46,47] These conclusions are completely consistent with activity data obtained from the polarization curves for CO bulk electrooxidation. Indeed, the current vs potential curves show that the as-prepared surfaces (Figure 2a′ and 3a′) are indeed the most active, with the activity in the preignition region being substantially higher than that on stepped surfaces (Figure 2c′ and 3c′).

The combined STM, CV, polarization, and IRAS measurements provide a consistent picture of the catalytic and morphological phenomena that underlie the polarization curves in Figure 1. As indicated by the STM-CV- ν_{CO} measurements, adislands on the as-prepared surfaces are gradually replaced by steps as the potential is cycled to progressively higher values (Figures 2−4). CO_2 intensities and polarization curves, in turn, show that these changes are accompanied by corresponding decreases in CO electrooxidation activity, also explaining the disappearance of the preignition peaks after the first potential cycle in Figure 1. The fact that steps induced by CO annealing show no activity for CO electrooxidation in the critically important preignition region is conclusively demonstrated by a comparison of Figures 2c′, 3c′, and 4; therein, it is clear that surfaces with

(35) Markovic, N.; Hanson, M.; McDougall, G.; Yeager, E. *J. Electroanal. Chem.* **1986**, *214*, 555–566.
(36) Kim, C. S.; Korzeniewski, C.; Tornquist, W. J. *J. Chem. Phys.* **1993**, *100*, 628–630.
(37) Kim, C. S.; Tornquist, W. J.; Korzeniewski, C. *J. Chem. Phys.* **1994**, *101*, 9113–9121.
(38) Kim, C. S.; Korzeniewski, C. *Anal. Chem.* **1997**, *69*, 2349–2353.
(39) Arenz, M.; Mayrhofer, K. J. J.; Stamenkovic, V.; Blizanac, B. B.; Tomoyuki, T.; Ross, P. N.; Markovic, N. M. *J. Am. Chem. Soc.* **2004**, *127*, 6819–6829.
(40) Friedrich, K. A.; Geyzers, K.-P.; Linke, U.; Stimming, U.; Stumper, J. *J. Electroanal. Chem.* **1996**, *402*, 123–128.
(41) Arenz, M.; Stamenkovic, V.; Wandelt, K.; Ross, P. N.; Markovic, N. M. *Surf. Sci.* **2002**, *506*, 287–296.
(42) Lin, W.-F.; Sun, S. G. *Electrochim. Acta* **1996**, *41*, 803–809.
(43) Zou, S.; Gomer, R.; Weaver, M. J. *J. Electroanal. Chem.* **2002**, *474*, 155–166.
(44) Gasteiger, H. A.; Markovic, N.; Ross, P. N.; Cairns, E. J. *J. Phys. Chem.* **1994**, *98*, 617–625.
(45) Gasteiger, H. A.; Markovic, N. M.; Ross, P. N. *Catal. Lett.* **1996**, *36*, 1–8.
(46) Grgur, B. N.; Markovic, N. M.; Ross, P. N. *J. Phys. Chem. B* **1998**, *102*, 2494–2501.
(47) Grgur, B. N.; Markovic, N. M.; Ross, P. N. *J. Electrochem. Soc.* **1999**, *146*, 1613–1619.

steps induced by CO annealing do not exhibit CO oxidation currents until the ignition potentials are reached. This result, in turn, shows that the remarkable activity of adislands cannot be attributed to the fact that the edges of large adislands may resemble "circular steps". Therefore, we propose that on low index Pt surfaces the unique properties of adislands must stem from fundamentally new chemical phenomena, perhaps occurring on the smallest adislands in our study (~0.5 nm in diameter); such phenomena are discussed in our theoretical treatment below. Taken together, the above results demonstrate that it is now possible to establish reactivity trends for active sites based on highly irregular surface features such as adislands, as opposed to simple, well-ordered single-crystal surfaces, thus opening up new possibilities for electrocatalyst manipulation and design.

Having determined that adislands are uniquely active for CO electrooxidation, it remains to establish a molecular-level catalytic explanation for this phenomenon. The adislands may serve as nucleation sites for OH groups. However, given that CO is also more strongly adsorbed on defects than on flat terraces,[48,49] it is not clear whether OH can compete favorably with CO for adisland adsorption sites. Further complicating these interpretive efforts is the fact that a broad distribution of adisland shapes and sizes, together with steps, is clearly present on both the Pt(100) and Pt(111) terraces (Figures 2 and 3); CO and OH, in turn, likely interact differently with each of these features, resulting in the broadening of the preignition peaks seen in the polarization curves (Figure 1). To begin to unravel the rich complexity of these interactions, we use Density Functional Theory (DFT) calculations to probe the energetics of CO, OH, and water interaction with three model systems. The systems—perfect Pt(111) terraces,[50−55] perfect Pt(211) steps,[56,57] and adatoms on Pt(111)—constitute very simple structural models of the experimentally studied platinum surfaces. The models do, however, capture the extremes in the rich distribution of surface sites on the experimental surfaces, ranging from the highly coordinated features on the adislands to the smoothest areas of the terraces.

On all of these surface features, we determine the differential free energies of CO adsorption from a saturated solution of CO and of OH from liquid water (see Experimental Section) at high CO coverages; the difference in these free energies serves as a very simple descriptor for the rate of CO electrooxidation.[58] We note that this descriptor, which gives the competition between OH and CO adsorption on a given type of surface site, is purely thermodynamic in nature; the inclusion of kinetic effects will likely favor undercoordinated features.[59] The difference in the calculated descriptor values on adatoms, steps, and terraces ("relative" descriptor values), in turn, gives an estimate of the relative rates of CO electrooxidation on these features.

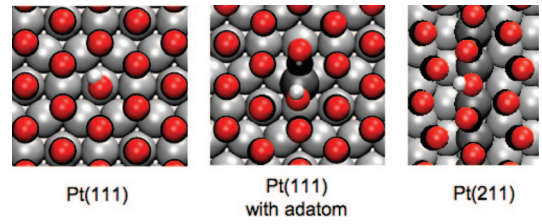

Figure 5. OH adsorption on CO-covered platinum surfaces. Red, black, white, and gray circles denote oxygen, carbon, hydrogen, and platinum atoms, respectively. A darker shade of gray is used to denote platinum adatoms or platinum atoms on the step edge of Pt(211). A stabilizing water bilayer on the adatom is not shown.

To model the effects of the near-saturation coverages of CO that will be found on platinum surfaces in CO-saturated solutions, we perform all of our calculations with the well-known (2 × 2)-3CO adstructure;[15,60] this structure represents the highest CO coverage observed in our experimental studies. On perfect Pt(111) terraces, and at a potential of 0.8 V vs SHE (a typical potential in the Pt(111) preignition region, Figure 1), we find that the most favorable site for OH adsorption (the top site) has an adsorption free energy of ~0.79 eV compared to liquid water; the differential CO adsorption free energy on the same sites is small (~ −0.19 eV), as one might expect at near-saturation CO coverages. On Pt(211) steps (again at high CO coverages), OH binds most favorably at bridge sites (~0.30 eV), as does CO (~ −0.46 eV). These results yield a relative descriptor value (i.e., the difference in Pt(211) and Pt(111) free energies of OH adsorption minus the corresponding difference for CO) of −0.22 eV, implying that steps are more active for CO electrooxidation than terraces are at 0.8 V. On terraces with Pt adatoms (representing highly undercoodinated features on the Pt adislands), it is thermodynamically favorable for two CO molecules to bind to a single adatom (Figure 5). The least strongly bound of these CO molecules is the most catalytically active and can be displaced by OH; in this case, the relative descriptor value (compared to perfect (111) terraces) is −0.30 eV. Here, in contrast to the results on (111) and (211) surfaces, we find that a stabilizing contribution from a water bilayer, determined on a (3 × 2) unit cell (see Supporting Information), is significant and substantially enhances the competitiveness of OH adsorption on the adatoms.

The above results suggest that, in a thermodynamic sense, OH can better compete with CO for sites on adatoms in CO-saturated solutions than it does on perfect terraces; the behavior on steps is intermediate between that on terraces and adatoms. The enhanced competition of OH for sites on adatoms (or on other highly undercoordinated features present on larger adislands) results both from the Pt−CO bond weakening, caused by the adsorption of two CO molecules on individual Pt adatoms, and from the stabilization of OH on adatoms by adjacent water bilayers; neither effect is present on pure steps

(48) Mavrikakis, M.; Baumer, M.; Freund, H. J.; Norskov, J. K. *Catal. Lett.* **2002**, *81*, 153–156.
(49) Remediakis, I. N.; Lopez, N.; Norskov, J. K. *Angew. Chem., Int. Ed.* **2005**, *44*, 1824–1826.
(50) Grabow, L.; Xu, Y.; Mavrikakis, M. *Phys. Chem. Chem. Phys.* **2006**, *8*, 3369–3374.
(51) Greeley, J.; Mavrikakis, M. *J. Phys. Chem. B* **2005**, *109*, 3460–3471.
(52) Tsuda, M.; Kasai, H. *Jpn. J. Appl. Phys., Part 2* **2006**, *45*, L1219–L1221.
(53) Gong, X. Q.; Raval, R.; Hu, P. *Phys. Rev. Lett.* **2004**, 93.
(54) Narayanasamy, J.; Anderson, A. B. *J. Electroanal. Chem.* **2003**, *554*, 35–40.
(55) Knudsen, J.; Nilekar, A. U.; Vang, R. T.; Schnadt, J.; Kunkes, E. L.; Dumesic, J. A.; Mavrikakis, M.; Besenbacher, F. *J. Am. Chem. Soc.* **2007**, *129*, 6485–6490.
(56) Creighan, S. C.; Mukerji, R. J.; Bolina, A. S.; Lewis, D. W.; Brown, W. A. *Catal. Lett.* **2003**, *88*, 39–45.
(57) Orita, H.; Inada, Y. *J. Phys. Chem. B* **2005**, *109*, 22469–22475.
(58) Liu, P.; Logadottir, A.; Norskov, J. K. *Electrochim. Acta* **2003**, *48*, 3731–3742.
(59) Norskov, J. K.; Bligaard, T.; Logadottir, A.; Bahn, S.; Hansen, L. B.; Bollinger, M.; Bengaard, H.; Hammer, B.; Sljivancanin, Z.; Mavrikakis, M.; Xu, Y.; Dahl, S.; Jacobsen, C. J. H. *J. Catal.* **2002**, *209*, 275–278.
(60) Lucas, C. A.; Markovic, N. M.; Ross, P. N. *Surf. Sci.* **1999**, *425*, L381–L386.

or terraces. These effects, combined with the enhanced kinetics of water activation that are also expected on adatoms,[38] in turn suggest that CO electrooxidation rates will be higher on adatoms than on steps or terraces. We note, in passing, that these results imply that, as small, highly undercoordinated adislands grow larger and develop more step-like edges and more terrace-like surfaces, their activity will decrease and will approach that of CO-annealing induced steps and terraces. These conclusions are fully consistent with the experimental observations, and taken together, the computational and experimental results provide a compelling picture of the unique chemistry occurring on highly undercoordinated features on adislands.

Conclusions

The present study demonstrates the capability of a broad range of techniques, including electrochemical (EC), scanning tunneling microscopy (STM), infrared adsorption spectroscopy (IRAS), and Density Functional Theory (DFT), to add a remarkable degree of atomic-level insight into the structure−function relationships at electrified solid-solution interfaces. We have used these approaches to demonstrate that adislands are uniquely active for bulk CO electrooxidation on platinum and can be stabilized under conditions relevant to this reaction. Careful synthesis and control of these and related adfeatures may, however, have applications well beyond the Pt−CO interface, including the design of more active and robust electrocatalysts for a variety of reactions relevant to fuel cells and clean energy production.

Acknowledgment. This work was supported by the contract (DE-AC02-06CH11357) between the University of Chicago and Argonne, LLC, and the U.S. Department of Energy. Use of the Center for Nanoscale Materials was supported by the U.S. Department of Energy, Office of Science, Office of Basic Energy Sciences, under Contract No. DE-AC02-06CH11357. We acknowledge computer time at the Laboratory Computing Resource Center (LCRC) at Argonne National Laboratory, The National Energy Research Scientific Computing Center (NERSC), and the Molecular Science Computing Facility (MCSF) at Pacific Northwest National Laboratory.

Supporting Information Available: Figures showing the role of OH_{ad} in Ar purged solution (Fugure S1), the structural details of $\sqrt{19}$ structure (Figure S2), histograms of average adisland perimeter distribution (Figures S3 and S4), band shapes of a-top CO (Figure S5), and methodological details of DFT calculations. This information is available free of charge via the Internet at http://pubs.acs.org.

JA8032185